CHIN. PHYS. LETT. Vol. 31, No. 11 (2014) 114208

Electron Beam Lithographic Pixelated Micropolarizer Array for Real-Time Phase Measurement *

ZHANG Zhi-Gang(张志刚)[1], DONG Feng-Liang(董凤良)[2], CHENG Teng(程腾)[1], QIAN Ke-Mao(钱克矛)[3], QIU Kang(仇康)[1], ZHANG Qing-Chuan(张青川)[1**], CHU Wei-Guo(褚卫国)[2**], WU Xiao-Ping(伍小平)[1]

[1]*CAS Key Laboratory of Mechanical Behavior and Design of Materials, Department of Modern Mechanics, University of Science and Technology of China, Hefei 230027*

[2]*Nanofabrication Laboratory, National Center for Nanoscience and Technology, Beijing 100190*

[3]*School of Computer Engineering, Nanyang Technological University, Singapore 639798, Singapore*

(Received 28 August 2014)

Pixelated micropolarizer arrays (PMAs) have recently been used as key components to achieve real-time phase measurement. PMA fabrication by electron beam lithography and inductively coupled plasma-reactive ion etching is proposed in this work. A 320 × 240 aluminum PMA with 7.4 μm pitch is successfully fabricated by the proposed technique. The period of the grating is 140 nm, and the polarization directions of each of the 2 × 2 units are 0°, 45°, 90°, and 135°. The scanning electron microscopy and optical microscopy results show that the PMA has a good surface characteristic and polarization performances. When the PMA is applied to phase-shifting interferometry, four fringe patterns of different polarization directions are obtained from only one single frame image, and then the object wave phase is calculated in real time.

PACS: 42.87.Bg, 42.25.Ja, 81.16.Nd DOI: 10.1088/0256-307X/31/11/114208

Phase-shifting interferometry techniques, including time the phase-shifting (TPS) technique[1–3] and the space phase-shifting (SPS) technique,[4–6] have been rapidly developed over the past few decades. However, the TPS requires precise vibration control and is limited to the measurement of static or quasi-static objects.[3] The SPS can be used in the dynamic measurement, while requires pixel-level position match and fringe intensity correction.[6] The application of a pixelated micropolarizer array (PMA) in the SPS technique overcomes the position match problem and greatly eases the SPS technique. Awatsuji *et al.*[7] first proposed the PMA-based SPS technique and then this technique is extensively researched[8,9] and used in real-time interferometry,[8,10] digital holography,[11] and three-dimensional microscopy.[12,13]

Depending on the polarization materials used, the PMAs are mainly divided into three types: the iodine-doped polyvinyl alcohol (PVA) layer,[14] the liquid crystals,[15] and the metal nano-grating.[16,17] The thickness of a PVA layer is about 10 μm, which is much larger than the pitch of the CCD unit.[14] The cross talk between the adjacent units then occurs, which reduces the measurement precision and accuracy. The extinction ratio of the PMA based on the liquid crystals is low in the red wave band, which limits the range of actual applications.[15] The thickness of metal nano-grating can reach about 100 nm, and the theoretical extinction ratio and transmittance are excellent in the visible wave band, making it suitable for practical applications.

Nanoimprint lithography shows good ability to fabricate the micropolarizer array and to integrate the PMA with other functional substrates,[18–20] which would be a good choice for volume production of PMA. To fabricate the PMA based on the nano-grating, multiple interferometric exposures and hierarchical etching the metal layer for different polarization direction units have been used.[17] This method has the following problems. (i) Field non-uniformity and field distortion of the exposure light source make the exposure intensities at different positions inconsistent. (ii) Hierarchical etching increases the metal layer thickness and the process complexity, and decreases the yield. (iii) Different layers have different performances.

To overcome the problems associated with the interference exposure, a better choice is to use electron beam lithography (EBL), which has been well developed and applied to grating fabrication.[21–23] The resist is exposed by an electron beam, and then the nanostructure is obtained after development. The increased EBL power improves the exposure speed, making it feasible for PMA fabrication. In detail, EBL has the following advantages. (i) The resolution is high, and exposure intensities at different positions are consistent. (ii) EBL has the advantage of less artificial operation compared with the multiple interferometric exposures, thus the exposure process difficulty is decreased. (iii) All polarizer units are etched in the same layer, thus the thickness is only a quarter of the one fabricated by hierarchical etching. (iv) All these polarizer units are etched simultaneously, making the performances consistent. (v) The yield is increased. Indeed, using EBL for PMA fabrication has been reported in Ref. [24], where only a 2 × 2 array was made.

*Supported by the National Basic Research Program of China under Grant No 2011CB302105, the National Natural Science Foundation of China under Grant Nos 11332010, 11102201, 11127201, 11472266 and 11372300, and the Instrument Developing Project of the Chinese Academy of Sciences under Grant No YZ201265.

**Corresponding authors. Email: zhangqc@ustc.edu.cn; wgchu@nanoctr.cn

© 2014 Chinese Physical Society and IOP Publishing Ltd

In this Letter, we report the successful fabrication of a large PMA (320 × 240) by EBL. To the best of our knowledge, the large PMA fabricated by EBL is reported for the first time. Furthermore, the fabricated PMA has been integrated onto the focal plane of a CCD to achieve real-time phase measurement.

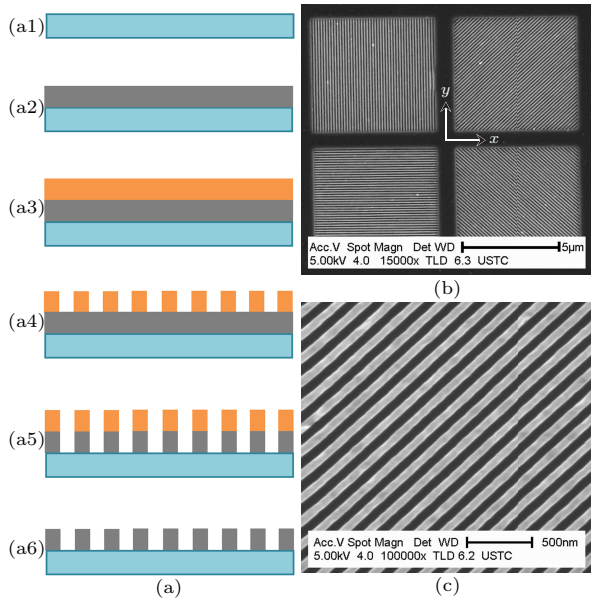


Fig. 1. Fabrication processes and SEM observation of PMA: (a) fabrication processes of PMA by EBL, (b, c) the SEM images of PMA at different magnifications.

During the PMA fabrication by EBL, aluminum is chosen as the metal material. The cross-sectional shape of the grating is rectangular, and the period, duty ratio and depth of the grating are 140, 0.5, 100 nm, respectively. The pitch of PMA units is 7.4 μm, which is the commonly used size of CCD. The surrounding of the units is a 1 μm wide opaque area to reduce the cross talk between adjacent units. The fabrication process is shown in Fig. 1(a) and explained as follows. Firstly, high transmittance glass is used as a substrate, and is double-side polished and cleaned. Secondly, a 100-nm-thick aluminum layer is deposited on the substrate. Thirdly, a layer of positive electron beam resist (ZEP 520) is spin-coated on the top of the aluminum layer. The resist is baked at 180℃. Fourthly, the resist layer is exposed by the electron beam exposure device (Vistec EBPG 5000+ ES), and then the nano-grating structure of four directions in the resist layer is obtained after development. Fifthly, the nano-grating structure is transferred from the resist layer to the aluminum layer by an inductively coupled plasma-reactive ion etching (ICP-RIE) device. Finally, the resist layer is removed.

Figures 1(b) and 1(c) show the scanning electron microscope (SEM) images of our fabricated PMA at magnifications of 15000× and 100000×, respectively. The polarizer units have a pitch of 7.4 μm, and isolated by a 1 μm wide aluminum frame isolation. The normal directions of the gratings are 0° (upper-left), 45° (lower-right), 90° (lower-left) and 135° (upper-right). Compared with the PMA fabricated by the interferometric exposures in Ref. [17], the grating lines are much straighter and have uniform thickness. An optical microscope is used to analyze the polarization characteristic of the PMA. The observation light is green. An electric precision rotating platform with a polarizer in the middle is placed in front of the light source. The polarization direction of the light is changed by rotating the polarizer. Figures 2(a)–2(d) show the partial images recorded by the optical microscope when the polarization directions of light are at 0°, 45°, 90°, and 135°, respectively.

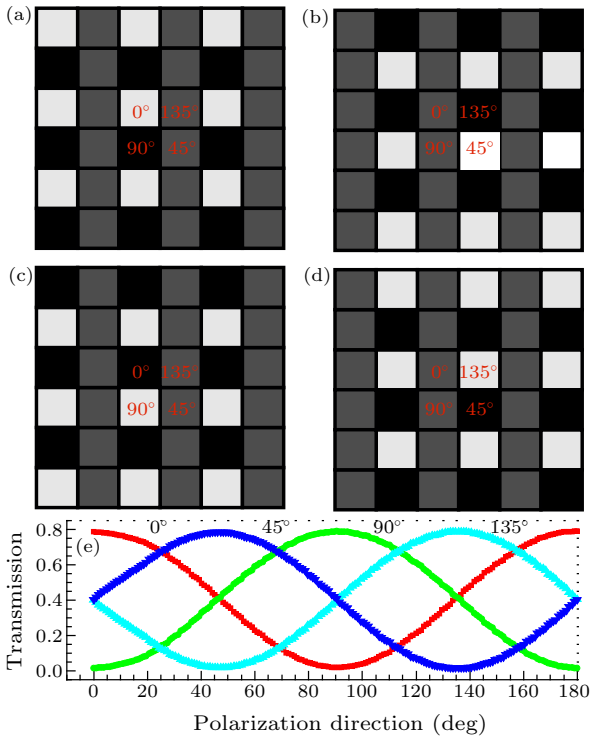


Fig. 2. Polarization performance of PMA. (a)–(d) The partial images recorded by an optical microscope when the polarization directions of the illumination light are at 0°, 45°, 90°, and 135°, respectively. (e) Transmittances changed with the polarization direction of the incident green light.

The maximum polarization transmittance and extinction ratio are calculated to evaluate the polarization performance of the PMA by using a 12-bit camera.[24] The offset degree of the recording frame is 1°. The transmittance curves of the 0°, 45°, 90°, and 135° units with the polarization direction of the incident light are shown in Fig. 2(e). The curves are in the forms of the trigonometric function distributions. For the 0°, 45°, 90°, and 135° units, the maximum polarization transmittances are 78.84%, 78.78%, 78.71%, and 78.70%, respectively, and the minimum polarization transmittances are 1.84%, 1.52%, 1.64%, and 1.70%, respectively. The extinction ratio is the ratio of the maximum polarization transmittance and the minimum polarization transmittance, which can be calculated to be 42.9, 51.8, 47.9, and 46.3, respectively. A good maximum polarization transmittance

and extinction ratio are obtained.

The fabricated PMA is then integrated onto a focal plane of a CCD (10 bits) with the same unit pitch as follows. Firstly, the dust-proof glass cover was removed from the CCD sensor device. Secondly, an ultraviolet curing adhesive was coated in the focal plane of the CCD sensor device. Thirdly, the PMA was placed on the CCD sensor device, with the aluminum layer of the PMA towards the CCD sensor. Fourthly, the CCD sensor is in a working state, and the illumination light was an adjustable linearly-polarized parallel light. The position and angle of the PMA were precisely adjusted to obtain the optimum extinction ratio of the image as captured by the CCD camera itself. Fifthly, ultraviolet light was used to cure the adhesive. Finally, the dust-proof glass cover was replaced back over the CCD sensor device.

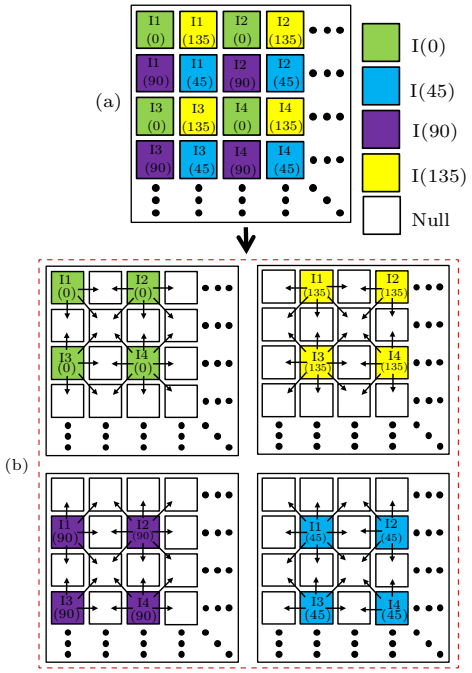


Fig. 3. Schematic diagrams of linear interpolation to obtain four images of different polarization directions. (a) A single frame image captured by the CCD integrated with PMA. (b) A linear interpolation method is used to obtain the four images.

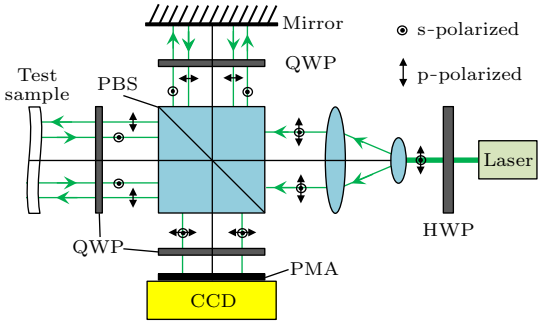


Fig. 4. The light path of phase-shifting interferometry.

To obtain four images of different polarization directions from a single frame image, a linear interpolation method is used, see Fig. 3. Figure 3(a) shows a single frame image captured by CCD, and then the gray values of the same polarization directions are copied to the same position of blank images with the same resolution, thereby four images are generated, see Fig. 3(b). Each of the four images has a quarter of original data and three quarters of null values. The null values are filled by using the linear interpolation method based on the adjacent original data. Therefore, four images of different polarization directions are obtained from a single frame image.

The PMA is applied to phase-shifting digital holography to measure the phase in real time. The interferometry light path is shown in Fig. 4. A 532 nm laser beam is split into two mutually perpendicular linear polarization beams by the polarization beam splitter (PBS): the p-polarized beam is transmitted to the test sample and the s-polarized beam is reflected to the mirror. A half wave plate (HWP) is used to adjust the intensity ratio of the two beams. When the two light beams recombine in the PBS, the polarization direction rotates 90° by transmitting the quarter wave plate (QWP) twice. After the combined beams transmit through the QWP and PMA, the fringe pattern is acquired by the CCD. Four images can be obtained from a single frame image, which represent the images of polarization directions at 0°, 45°, 90°, and 135°, and the gray value can be expressed as $I(0)$, $I(45)$, $I(90)$, and $I(135)$. The interference light intensity is related to the polarization angle of the PMA unit,

$$I(\alpha) = \frac{1}{2}[I_{\rm s} + I_{\rm r} + 2\sqrt{I_{\rm s}I_{\rm r}}\cos(\varphi + 2\alpha)], \quad (1)$$

where $I_{\rm s}$ is the object beam intensity, $I_{\rm r}$ is the reference beam intensity, φ is the object beam phase, and α is the polarization angle of the PMA unit. Thus the light intensity of the four polarization direction images can be expressed as follows:

$$I(0) = \frac{1}{2}[I_{\rm s} + I_{\rm r} + 2\sqrt{I_{\rm s}I_{\rm r}}\cos(\varphi)], \quad (2)$$

$$I(45) = \frac{1}{2}[I_{\rm s} + I_{\rm r} + 2\sqrt{I_{\rm s}I_{\rm r}}\cos(\varphi + \pi/2)], \quad (3)$$

$$I(90) = \frac{1}{2}[I_{\rm s} + I_{\rm r} + 2\sqrt{I_{\rm s}I_{\rm r}}\cos(\varphi + \pi)], \quad (4)$$

$$I(135) = \frac{1}{2}[I_{\rm s} + I_{\rm r} + 2\sqrt{I_{\rm s}I_{\rm r}}\cos(\varphi + 3\pi/2)]. \quad (5)$$

The object phase can be calculated from the above equations,

$$\varphi = \arctan\left[\frac{I(135) - I(45)}{I(0) - I(90)}\right]. \quad (6)$$

The size of the measureable area is about 2.4 mm × 1.8 mm.

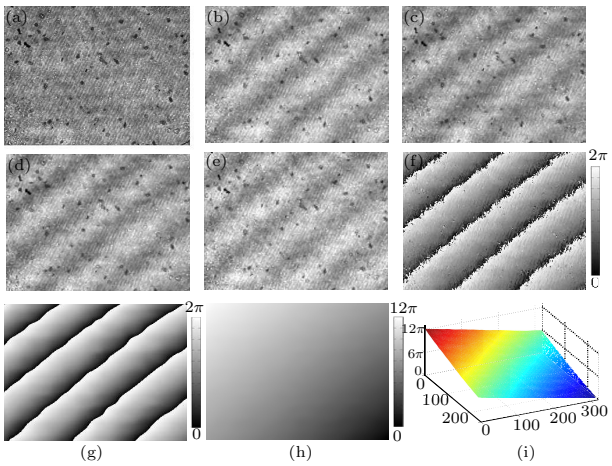


Fig. 5. The application of the PMA to measure the slightly tilted plane wave phase. (a) A single frame image captured by the CCD integrated with PMA; (b)–(e) images at 0°, 45°, 90°, and 135° obtained from (a) by the linear interpolation method; (f) wrapped phase image; (g) wrapped phase filtered by WFT; (h) unwrapped phase image of (g); and (i) three-dimensional display of unwrapped phase (h). The unit of the x-axis/y-axis is in pixels.

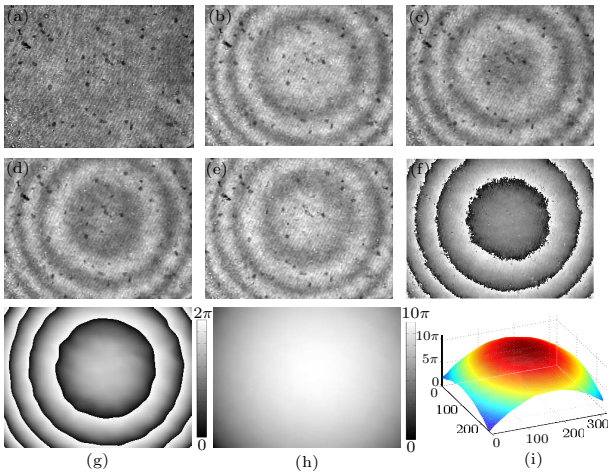


Fig. 6. The application of the PMA to measure the spherical wave phase. (a) A single frame image captured by the CCD integrated with PMA; (b)–(e) images at 0°, 45°, 90°, and 135° obtained from (a) by the linear interpolation method; (f) wrapped phase image; (g) wrapped phase filtered by WFT; (h) unwrapped phase image of (g); and (i) three-dimensional display of unwrapped phase (h). The unit of the x-axis/y-axis is in pixels.

Figure 5 is the application of the PMA in the phase-shifting interferometry to measure a slightly tilted plane wave phase. The test sample is a smooth flat plane, and the normal direction is adjusted to have a slight tilt along the incident light. A single frame image is captured, see Fig. 5(a). Some black spots are observed, which are caused by dust in the air adhered to the focal plane of the CCD introduced in the integration process. They can be eliminated when the integration is carried out in a clean room in our future work. Four fringe patterns are obtained from Fig. 5(a) by the linear interpolation method, as shown in Figs. 5(b)–5(e). Then the unwrapped phase is calculated, as shown in Fig. 5(f). As the black spots are not completely opaque, the influence of the black spot is weak, while the noise is obvious. To filter the noise, windowed Fourier transform (WFT) is applied to the phase map,[25] with a filtered result shown in Fig. 5(g). The subsequent unwrapping gives the result in Fig. 5(h), which is also shown in the three-dimensional display in Fig. 5(i). The measured phase is slightly tilted and is consistent with the actual setting. More quantitative evaluation will be carried out further.

Figure 6 is the application of the PMA in the phase-shifting interferometry to measure the spherical wave phase. The test sample is a smooth concave mirror. A single frame image is captured, see Fig. 6(a). Then four fringe patterns are obtained, see Figs. 6(b)–6(e). Figures 6(f)–6(i) are the wrapped phase, wrapped phase filtered by WFT, unwrapped phase, and the three dimensional display of the unwrapped phase, respectively. The measured phase is the spherical wave phase, as is expected.

In conclusion, a 320 × 240 PMA fabricated by EBL and ICP-RIE is described. The four polarization direction units are placed in one layer, resulting in the uniform grating structure and consistent polarization performance for the four different grating direction units. The PMA is applied to the real-time phase-shifting interferometry, and the phase image can be calculated from a single frame image. This method would greatly widen applications of the phase-shifting technology, such as dynamic interferometry, and three-dimensional digital holographic microscopy of living cells.

References

[1] Bruning J H et al 1974 *Appl. Opt.* **13** 2693
[2] Kato J et al 1993 *Appl. Opt.* **32** 77
[3] Zhang Z et al 2013 *Opt. Eng.* **52** 103109
[4] Haasteren A J P and Frankena H J 1994 *Appl. Opt.* **33** 4137
[5] Kujawinska M and Robinson D W 1988 *Appl. Opt.* **27** 312
[6] Qian K et al 1999 *Opt. Lasers Eng.* **31** 289
[7] Sasada M et al 2004 *International Commission for Optics* (Chiba) pp 187 357
[8] Millerd J et al 2004 *Proc. SPIE* **5531** 304
[9] Awatsuji Y et al 2004 *Appl. Phys. Lett.* **85** 1069
[10] Brock N J et al 2011 *Proc. SPIE* **8160** 81600W
[11] Tahara T et al 2012 *Opt. Lett.* **37** 4002
[12] Tahara T et al 2010 *Biomed. Opt. Express* **1** 610
[13] Creath K and Goldstein G 2012 *Biomed. Opt. Express* **3** 2866
[14] Gruev V et al 2007 *Opt. Express* **15** 4994
[15] Zhao X et al 2011 *Opt. Express* **19** 5565
[16] Nordin G P et al 1999 *J. Opt. Soc. Am.* A **16** 1168
[17] Gruev V 2011 *Opt. Express* **19** 24361
[18] Ahn S H et al 2007 *J. Vac. Sci. Technol.* B **25** 2388
[19] Chu J K et al *IEEE Photon. Technol. Lett.* **26** 469
[20] Chu J K et al 2013 *J. Micro-Nanolith MEM* **12** 033005
[21] Zhao Y R et al 2014 *Exp. Mech.* **54** 45
[22] Xie H M et al 2000 *Opt. Laser Technol.* **32** 361
[23] Kishinoto S and Egashira M 1993 *Opt. Eng.* **32** 522
[24] Gao S et al 2013 *Proc. SPIE* **8873** 88730L
[25] Qian K 2007 *Opt. Lasers Eng.* **45** 304